Received: 11 January 2019 | Revised: 28 June 2019 | Accepted: 17 July 2019

DOI: 10.1002/dep2.86

ORIGINAL RESEARCH ARTICLE

The Depositional Record Open Access
A journal of the International Association of Sedimentologists
WILEY

# Turbulent diffusion modelling of sediment in turbidity currents: An experimental validation of the Rouse approach

**Joris T. Eggenhuisen**[1] | **Mike C. Tilston**[1] | **Jan de Leeuw**[1] | **Florian Pohl**[1] | **Matthieu J. B. Cartigny**[2]

[1]Department of Earth Sciences, Utrecht University, Utrecht, the Netherlands

[2]Department of Geography, Durham University, Durham, UK

**Correspondence**
Joris T. Eggenhuisen, Room 288, Vening Meinesz Building A, Princetonlaan 8a, 3584 CB Utrecht, the Netherlands.
Email: j.t.eggenhuisen@uu.nl

**Funding information**
Equinor; Exxon Mobil Corporation; Nederlandse Organisatie voor Wetenschappelijk Onderzoek, Grant/Award Number: 864.13.006; Shell

## Abstract

The margins of submarine channels are characterized by deposits that fine away from the channel thalweg. This grain-size trend is thought to reflect upward fining trends in the currents that formed the channels. This assumption enables reconstruction of turbidity currents from the geologic record, thereby providing insights into the overall sediment load of the system. It is common to assume that the density structure of a turbidity current can be modelled with simple diffusion models, such as the Rouse equation. Yet the Rouse equation was developed to describe how particles should be distributed through the water column in open-channel flows, which fundamentally differ from turbidity currents in terms of their flow structure. Consequently, a rigorous appraisal of the Rouse model in deep-marine settings is needed to validate the aforementioned flow reconstructions. The present study addresses this gap in the literature by providing a robust evaluation of the Rouse model's predictions of vertical particle segregation in two experimental turbidity currents that differ only in terms of their initial bed slopes (4° versus 8°). The concentration profiles of the coarsest sediment, which is suspended predominantly in the lower part of the flow, is accurately reproduced by the Rouse equation. Significant mismatches appear, however, in the concentration of finer grained sediment, especially towards the top of the flow. This problem is caused by the mixing with clear water at the top of turbidity currents. Caution is therefore advised in applying a Rouse model to levee overspill and levee-crest deposits. Nonetheless, the Rouse model shows good agreement with laboratory measurements in the lower regions of the flow and for the coarser grains that are predominantly transported in the lower sections of submarine channels.

**KEYWORDS**

Grain-size segregation, Rouse modelling, simplified sediment transport modelling, turbidity current reconstruction

## 1 | INTRODUCTION

Grain-size stratification is a common feature of turbidity currents (Straub and Mohrig, 2008; Kane and Hodgson, 2011; Hansen *et al.*, 2015). Sand-rich channel fills and clay-rich levees of submarine channels can therefore be deposited by the same flows (Hiscott *et al.*, 1997). Vertical grain-size gradients in turbidity currents have been measured in flume experiments (Garcia, 1994; Baas *et al.*, 2005; Straub and Mohrig, 2008; Straub *et al.*, 2011), and modelled with numerical models (Stacey and Bowen, 1988; Huang *et al.*, 2007; Abd El-Gawad, Cantelli, *et al.*, 2012; Abd El-Gawad, Pirmez, *et al.*, 2012). These vertical trends in the flow have also been reconstructed by analysing deposits from different elevations above the thalweg of channels and canyons (Hiscott *et al.*, 1997; Pirmez and Imran, 2003; Dennielou *et al.*, 2006; Babonneau *et al.*, 2010; Paull *et al.*, 2010; Migeon *et al.*, 2012; Hubbard *et al.*, 2014; Jobe *et al.*, 2017; Symons *et al.*, 2017). Figure 1 shows the deposit grain size versus height above the thalweg in a number of natural channel systems. These systems all have different characteristic flow thickness, and the range of sediment grain sizes available is different in each system, but all systems show a systematic decrease in deposit grain size with height above the thalweg of the channel or canyon.

These vertical grain-size gradients are the result of differences in vertical mixing between coarse and fine sediment fractions. In a current with a polydisperse sediment load (i.e. multiple sediment grain sizes), the coarse sediment fraction is concentrated near the base of the current, while finer sediment fractions are more homogenously distributed over the height of the current (Figure 2A; Garcia, 1994; Kneller and Buckee, 2000; Baas *et al.*, 2005; Hansen *et al.*, 2015; Tilston *et al.*, 2015). Intense turbulence will homogenize sediment of all grain sizes and will therefore reduce the vertical variation in grain size in turbidity currents (Baas *et al.*, 2005; Figure 2B). The grain-size gradient in a turbidity current, measured either directly or reconstructed from deposits, thus reflects important current properties.

Consequently, these deposits are increasingly being used as control points for the reconstruction of historic and ancient

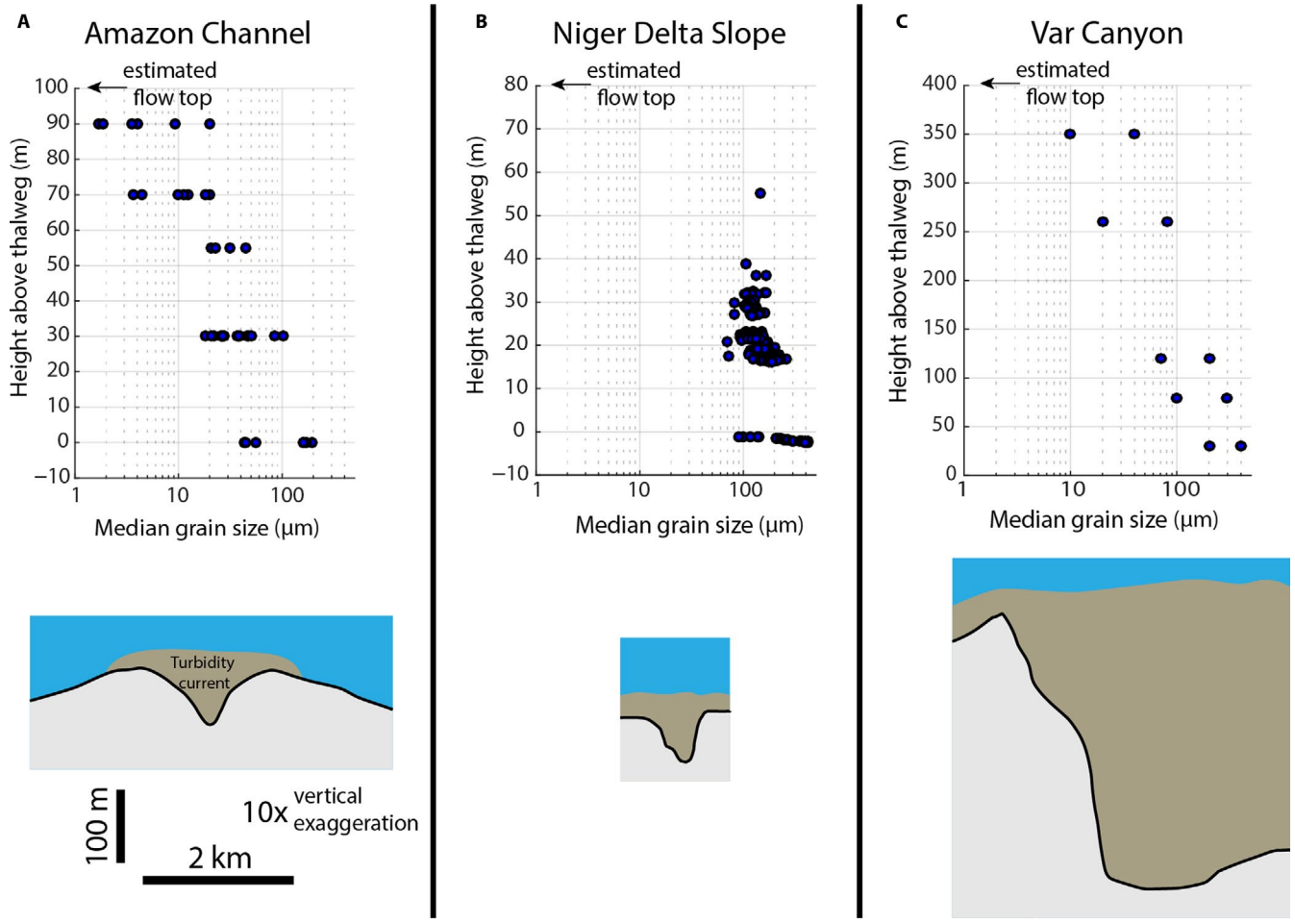


**FIGURE 1** Change in deposit grain size as a function of height above the channel thalweg for a number of natural submarine channels. (A) Amazon Channel (Hiscott et al., 1997; Pirmez and Imran, 2003). (B) Niger Delta Slope (Jobe et al., 2017). (C) Var Canyon (Migeon et al., 2012). A representative channel/canyon cross-section is shown for each of the systems. These cross-sections each have the same scale.

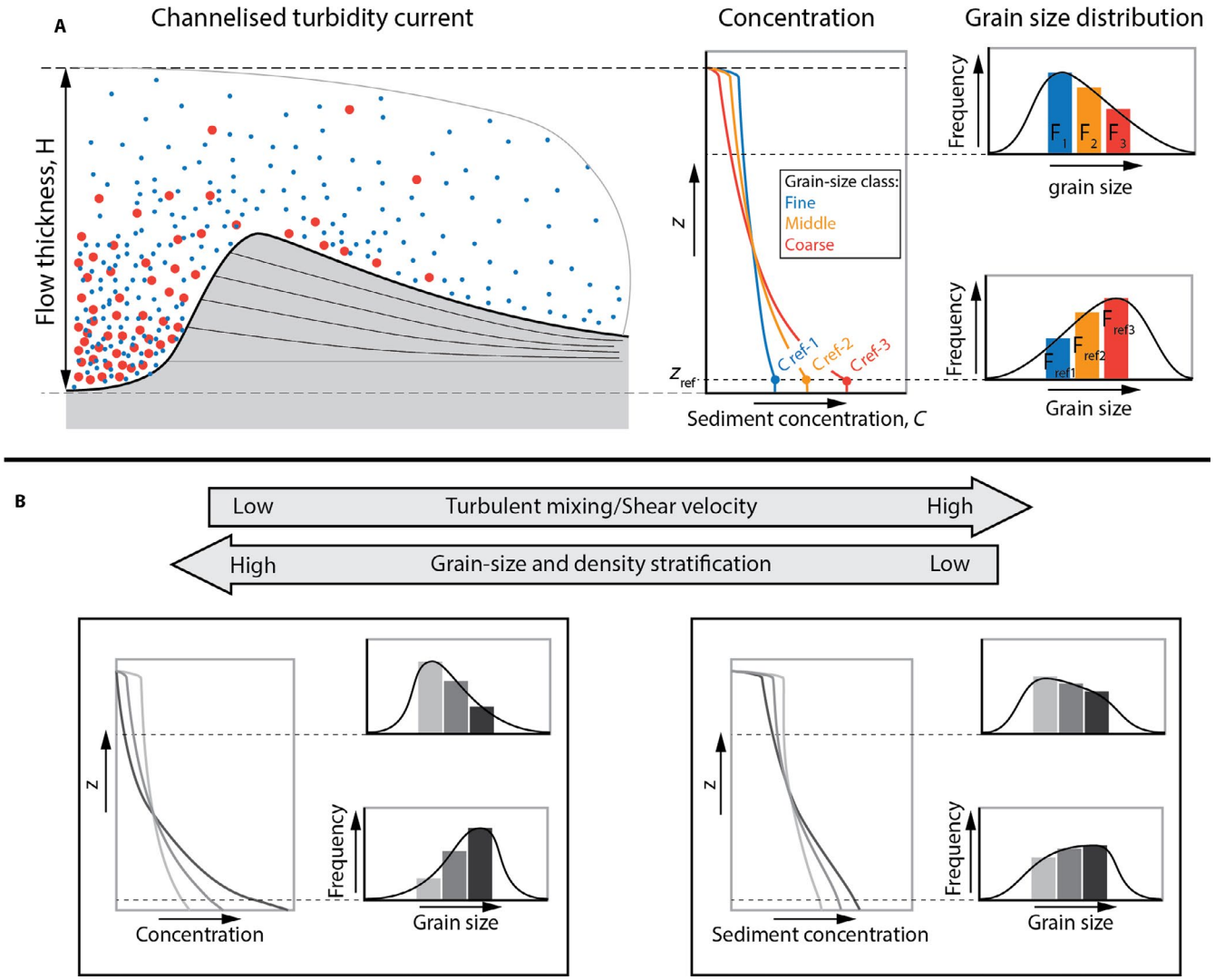


**FIGURE 2** Conceptual model of grain-size stratification in channelised turbidity currents. (A) Left: schematic representation of a leveed channel. Middle: concentration profiles for different grain-size classes. Right: grain-size distribution of suspended sediment at two levels in the flow. The coarse sediment fraction is concentrated near the base of the flow whereas the fine sediment fraction is more homogeneously mixed. The fine sediment fraction is therefore relatively more abundant in the upper part of the flow. Representation of fine and coarse-grained sediment in a channelised turbidity current adapted from Hansen *et al*. (2015). (B) In a Rousean model, turbidity currents become less stratified in grain size and density as the turbulent mixing intensity increases

turbidity current flow events in simplified modelling approaches. These approaches commonly rely on the classic equation for suspended sediment profiles in open-channel flow, as proposed by Rouse (1937), to describe grain-size stratification in turbidity currents (Hiscott, 1994; Hiscott *et al.*, 1997; Straub and Mohrig, 2008; Bolla Pittalua and Imran, 2014; Jobe *et al.*, 2017; Bolla Pittaluga *et al.*, 2018). In the Rouse equation, sediment particles are considered to be mixed by turbulence in analogy to heat, momentum and dissolved matter (Rouse, 1937; Vanoni, 1946; Graf, 1971; van Rijn, 1993; Vanoni, 2006; Garcia, 2008). An equilibrium concentration profile is reached when there is a balance between the upward flux due to turbulent mixing and the downward flux due to sediment settling. Many adjustments to the original Rouse model have been proposed since the 1937 publication (see textbooks and reviews by Vanoni, 1946; Graf, 1971; van Rijn, 1993; Vanoni, 2006; Garcia, 2008). We collectively refer to this family of equations, formulations and models as the Rousean approach. If valid, the Rousean approach represents a significant tool for the reconstruction of fluxes of sediment through submarine canyons and channels into deep-marine basins. However, the ability of Rousean models to accurately reproduce the density structure of turbidity currents has not been the subject of rigorous scrutiny yet.

The aim of this study is to validate the use of the Rouse equation as a simplification of the vertical grain size and density structure of turbidity currents. This aim will be achieved by comparing vertical profiles of concentration and grain size

obtained from experimental turbidity currents with results from an analytical model based on the Rouse equation.

## 2 | METHODS

### 2.1 | Grain-size stratification model

The classic formulation for the vertical distribution of suspended sediment concentration was proposed by Rouse (1937). The derivation is based on the analogy between the diffusion of heat, mass and velocity due to turbulence and the turbulent diffusion of suspended sediment particles. The turbulent diffusion will work to move sediment upwards, against the gradient of suspended sediment concentration. This can be understood by considering the action of upward and downward moving patches of fluid and sediment: the upwards movements will carry higher-concentration mixtures up; and the downwards movements will carry lower-concentration mixtures down. On average this results in a net flux that would homogenize the flow in the absence of gravity or for neutrally buoyant sediment. Gravity, however, pulls sediment with density larger than that of water downwards, resulting in a settling flux. Steady concentration profiles arise when the turbulent flux and the settling flux are in balance throughout the fluid column. Rouse evaluated this equilibrium, and the resulting equation gives the concentration profile of sediment in the grain-size class $i$ as (Rouse, 1937; see Garcia, 2008 for a modern treatment of the derivation):

$$C_i(z) = C_{\mathrm{refi}} \left( \frac{H-z}{z} \left( \frac{z_{\mathrm{ref}}}{H-z_{\mathrm{ref}}} \right) \right)^{\frac{v_{\mathrm{si}}}{\beta \kappa u^*}}, \qquad (1)$$

where $C_{\mathrm{refi}}$ is the volumetric concentration of suspended sediment (–) in grain-size class $i$ at the reference level $z_{\mathrm{ref}}$ (m), $H$ the thickness of the flow (m), $z$ the height above the bed (m), $v_{\mathrm{si}}$ the settling velocity of the sediment in grain-size class $i$ (m/s) (here taken to be positive), $\kappa$ is the von Karman constant (0.4) and $u^*$ is the shear velocity (m/s). Figure 2A shows a schematic concentration profile in which $H$, $z$, $z_{\mathrm{ref}}$ and $C_{\mathrm{refi}}$ are annotated for clarification of these parameters.

A number of key assumptions are made in the derivation of Equation 1. Firstly, it relies on the assumption of fully developed flow that is both steady in time and uniform in space. This is required because the Rouse equation depends on the balance between two processes, which takes time to establish. It can be argued, however, that the approach still holds in cases where the flow changes gradually in time and space, such that the timescales of change are longer than the timescales associated with settling and turbulent mixing (Bolla Pittaluga *et al.*, 2018).

Secondly, the diffusivity for sediment particles is assumed to be equal to the turbulent diffusivity. Differences between these diffusivities have been addressed by adding a proportionality constant commonly denoted as $\beta$ (van Rijn, 1993). This constant appears in the exponent of Equation 1. Conflicting effects of the interaction between turbulence and particles have been addressed in the literature. On the one hand, particles could spend less time in turbulent eddies due to settling compared to the fluid in the eddy, which reduces the effect of turbulent diffusion (Garcia, 2008). This can be accounted for by decreasing the value of $\beta$ to values smaller than 1. On the other hand, particles might be more effectively mixed by eddies when they are moved to the outside of eddies due to centrifugal effects (van Rijn, 1993). This can be accounted for in Equation 1 by increasing the value of $\beta$ to a value just above 1. It is common practice to set the value of $\beta$ to 1 (Garcia, 2008), or to at least not deviate too far from 1 because the physics of the interaction between particles and eddies is too complex and not well enough understood to parameterize it within the Rouse equation. A value of 1 will be used throughout this paper.

Thirdly, the diffusivity is assumed to obey a quadratic distribution with elevation above the bed, going to zero close to the bed and at the top of the flow, and with a maximum diffusivity at mid-flow depth.

All three of these assumptions have been discussed at length for the application of Equation 1 to open-channel flow. See van Rijn (1993) and Garcia (2008) for reviews of suggested modifications that can increase the accuracy of the classic formulation of the Rouse equation. Notwithstanding these potential improvements, the classic formulation is still found to be a satisfactory approximation of the suspended sediment concentration in a surprisingly broad range of laboratory and real-world open-channel flows, leading to a reputation as "one of the most important milestones in the field of sediment transport" (Garcia, 2008). Moreover, Bolla Pittaluga and Imran (2014) found that modifications to the classic formulation did not significantly impact the results of predicted concentration profiles for turbidity currents. Therefore, only the classic formulation will be used in this paper, with attention shifted to test the critical assumption for the application of the Rouse equation to turbidity currents: that it performs equally well for turbidity currents as it does for open-channel flow.

A simple model is constructed around the Rouse equation to test this assumption. The model requires four inputs related to the conditions of a specific turbidity current: (a) grain-size distribution of the suspended sediment at one reference level, (b) sediment concentration at the same reference level, (c) thickness of the flow and (d) the shear velocity of the flow. In principle, the reference level can be located anywhere in the flow where particle size and concentration are known.

The complexities of changing grain-size distributions and concentration curves with elevation require tracking of the

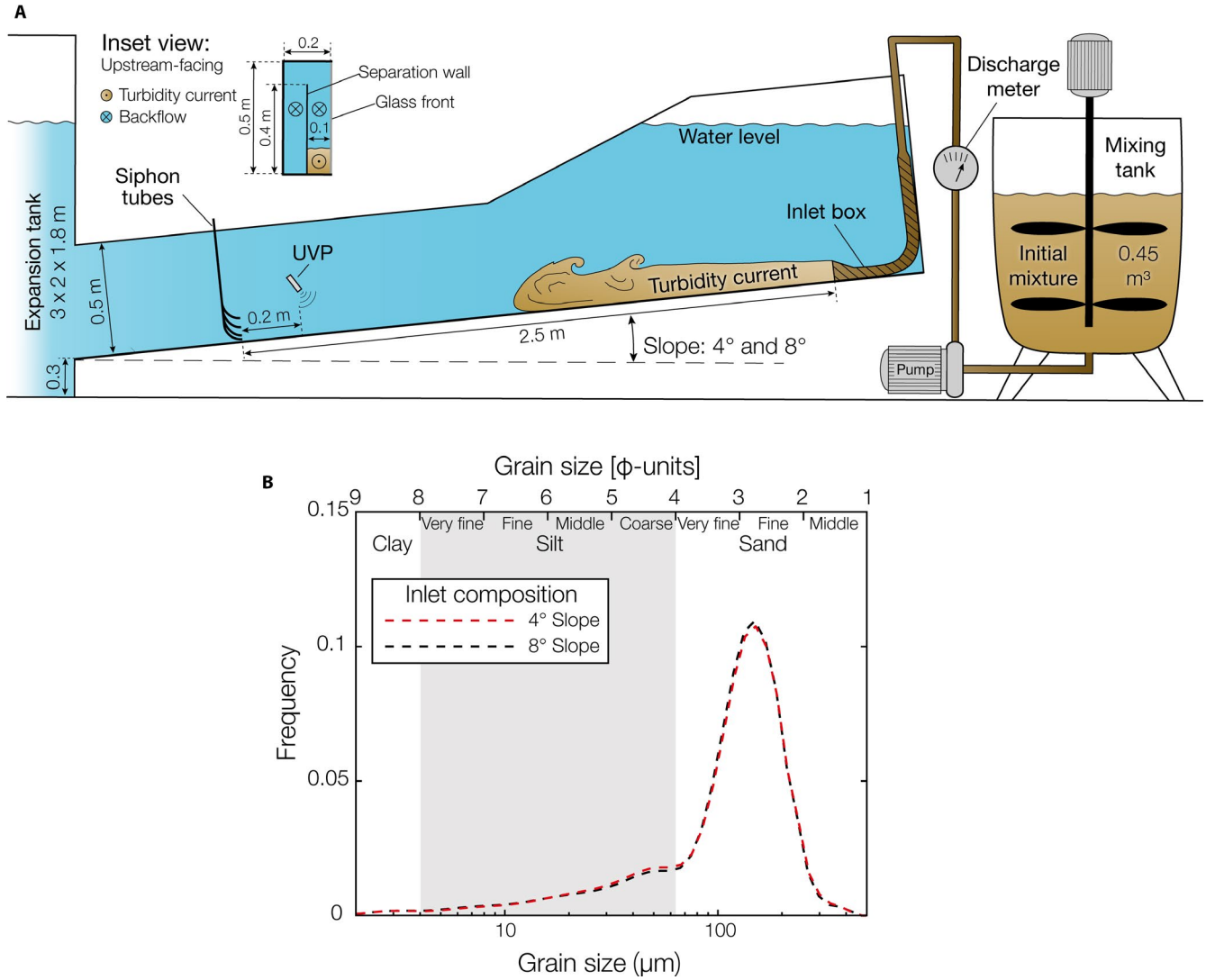


**FIGURE 3** (A) Sketch of the experimental setup. (B) Grain-size distributions of the sediment used in the two experiments

different grain-size classes and their concentrations at different elevations in the flow (Figure 2A). $C_{\text{refi}}$ is related to the total concentration at the reference level $C_{\text{ref}}$ as:

$$C_{\text{refi}} = C_{\text{ref}} F_{\text{refi}}, \tag{2}$$

where $F_{\text{refi}}$ is the fraction of the sediment volume at the reference level in grain-size class $i$. $F_{\text{refi}}$ is obtained from the grain-size analysis of a sediment sample from the reference level (Figure 2A).

The total sediment concentration profile is obtained by summation of the concentration profiles for the individual grain-size classes:

$$C(z) = \Sigma_i C_i(z) \tag{3}$$

The fraction of sediment in grain-size class $i$ at an elevation $z$ in the flow is obtained by dividing the concentration of sediment in class $i$ by the total concentration:

$$F_i(z) = \frac{C_i(z)}{C(z)} \tag{4}$$

The fraction of sediment in each grain-size class ($F_i$) is used to construct the grain-size distribution histogram of the suspended sediment at each height in the flow (Figure 2A). The grain-size distribution histograms are used to determine the 10$^{\text{th}}$, 50$^{\text{th}}$ and 90$^{\text{th}}$ percentile of the grain-size distribution ($D_{10}$, $D_{50}$ and $D_{90}$) at each elevation in the flow.

## 2.2 | Experimental setup

The analytical model is validated by comparing simulated vertical distributions of grain size to the sediment load observed in two experimental turbidity currents. For this analysis, two experiments were selected that were presented as part of a larger data set by Pohl *et al.* (2019). The experimental setup and procedure are based largely on Cartigny *et al.* (2013).

**TABLE 1** Boundary conditions and flow parameters during the flume experiments

| Run | Slope (tangent; degrees) | Initial sediment concentration (% vol.) | Discharge ($dm^3/s$) | Duration (s) | Depositional/non-depositional | Flow thickness (m) |
|---|---|---|---|---|---|---|
| 1 | 0.14; 8 | 17% | 3.5 | 115 | Non-depositional | 0.073 |
| 2 | 0.070; 4 | 17% | 3.5 | 115 | Depositional | 0.077 |

**TABLE 2** Acquisition settings for the UVP measurements

| | |
|---|---|
| Manufacturer and type | MET-FLOW; DUO MX |
| Speed of sound in water (m/s) | 1,480 |
| Measurement window (mm) | 175.38 |
| Number of channels | 238 |
| Distance between channel centres (mm) | 0.74 |
| Channel width (mm) | 3.7 |
| Frequency of the ultrasound beam (mHz) | 1 |
| Number of cycles per pulse | 5 |
| Number of sound pulses per measurement | 32 |
| Minimum on-axis velocity (mm/s) | −1,516.4 |
| Maximum on-axis velocity (mm/s) | 1,504.5 |
| On-axis velocity resolution (mm/s) | 11.8 |
| Pulse repetition frequency (kHz) | 4.1 |

### 2.2.1 | Setup and procedure

A mixture of sediment and fresh water with a volume of 0.45 $m^3$ was prepared in a mixing tank (Figure 3A). The grain size of the sediment was measured with a laser particle sizer (Malvern Mastersizer 2000™, https://www.malvernpanalytical.com; Figure 3B). The density of the sediment was 2,650 $kg/m^3$. The sediment concentration in the mixture was set to 17% vol. for both experiments, which resulted in a bulk mixture density of 1,280 $kg/m^3$. The mixture was pumped into the flume tank through a 4 m long pipe (diameter = 0.06 m) with a radial-flow pump and monitored by a discharge meter (Krohne® Optiflux 2300; https://uk.krohne.com). The discharge was set to 12.5 ± 0.7 $m^3/h$, resulting in a mean flow velocity of 0.81 ± 0.04 m/s in the inlet box and a flow duration of ~100 s.

The experiments were conducted in a 4 m × 0.5 m × 0.21 m flume tank (length × height × width; Figure 3A). The slope of the flume floor was adjusted to 4° and 8° in the two experiments respectively (see Table 1 for an overview of the boundary conditions of the two experiments). A longitudinally oriented separation wall subdivided the flume tank into two, 0.1 m wide channels (see inset view in Figure 3A). This measure was taken to minimize the effect of backflow during the experiments. Sediment with an identical grain size to the sediment used in the turbidity currents was glued to the flume floor to create a rough, non-erodible substrate. The turbidity currents left the flume through a free overfall into an expansion tank (3 m × 2 m × 1.8 m, with a floor 0.3 m lower than the flume tank floor). The currents could expand freely in the expansion tank and produced only a weak reflection wave which was too slow to travel back into the experimental setup during the experiment. Both the flume and expansion tank were filled with fresh water.

### 2.2.2 | Data Acquisition

A velocity profile was measured 2.3 m downstream of the inlet box with a Met-Flow UVP-Duo (https://www.met-flow.com). The UVP probe was positioned 0.11 m above the bed, angled 60° relative to the local bed slope (Figure 3A). The UVP data acquisition settings are provided in Table 2. The UVP measures velocities of the suspended particles in the direction of the beam axis. This measured velocity is converted into a bed-parallel component with the assumption that the bed-normal component is ~0 m/s, which is suitable for bypass conditions (Sequeiros *et al.*, 2018). A time-averaged velocity profile was calculated for the body of the current, which is associated with steady-flow conditions. The start of this averaging window was set to ~10 s after the current head passed the measurement location. The duration of the time-averaging was ~80 (s) (which was ~10 s before the end of the experiment).

Samples of suspended sediment were collected by siphoning off the turbidity current, 2.5 m downstream of the inlet (i.e. 0.2 m downstream of the UVP probe), at four different elevations above the flume tank floor (0.01, 0.02, 0.04 and 0.08 m; Figure 3A). The siphon-tube diameter was 7 mm and the average flow velocity in the tube was set to approximately 1 m/s, similar to the velocity scale of the turbidity current. Siphoning commenced ~10 s after the turbidity current entered the flume tank, after the current head passed through, and was continued until $2 \times 10^{-3}$ $m^3$ of mixture was sampled. The volume and weight of each siphon-tube sample were measured, and sediment concentration was calculated from the bulk density of the sample and the specific densities of the water and sediment. The grain-size distribution of the sampled sediment was subsequently analysed in the laser particle sizer.

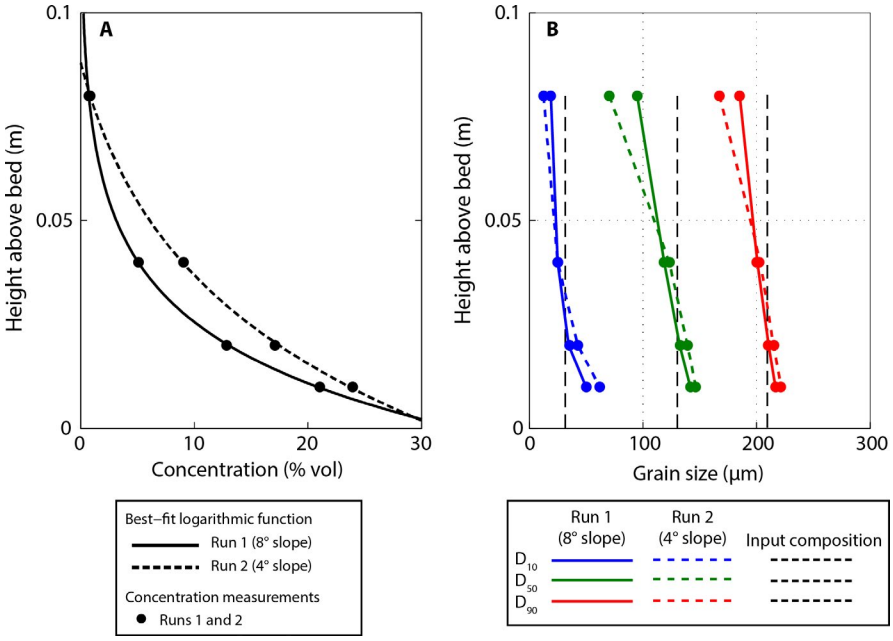


**FIGURE 4** (A) Sediment concentration profiles of Run 1 (8° flume floor slope) and Run 2 (4° flume floor slope). (B) Grain-size profiles of Run 1 and 2. Note that a steeper flume floor slope is associated with less vertical variation in grain size

### 2.2.3 | Data processing for model simulation

The grain-size distribution and sediment concentration at some reference level ($z_{ref}$) in the flow are obtained from the siphon samples. The lowermost siphoning tube at 0.01 m above the flume floor is chosen as the reference level.

The thickness of the flow ($H$) is here calculated using the integral method of Ellison and Turner (1959). This method defines the unknown thickness of a turbidity current, its unknown average bed-parallel velocity ($U$), and the square of the average velocity as a function of two integrals obtained from a velocity profile:

$$UH = \int_0^\infty \overline{u(z)}\mathrm{d}z \tag{5}$$

$$U^2H = \int_0^\infty \overline{u(z)}^2\,\mathrm{d}z \tag{6}$$

where $\overline{u(z)}$ is the time-averaged bed-parallel velocity (m/s) as a function of height above the bed, which is here obtained from the UVP measurements. Following the evaluation of the integrals with the UVP measurements, $U$ can be obtained by dividing Equation 6 by Equation 5. $H$ can then be determined by dividing Equation 5 by $U$.

The shear velocity of the two experimental turbidity currents is obtained with (Kneller, 2003):

$$u^* = \sqrt{g\frac{\Delta\rho}{\rho}H_{\mathrm{u\,max}}S}, \tag{7}$$

where $H_{\mathrm{umax}}$ is the height of the velocity maximum above the bed (m). $H_{\mathrm{umax}}$ can be evaluated from the UVP measurements. $\Delta\rho$ is the density difference between the turbidity current and the ambient fluid of density $\rho$ (kg/m$^3$). $\Delta\rho$ is calculated for the depth interval between the bed and the velocity maximum. To do this, best-fit logarithmic functions were determined for the concentrations measured in the siphon samples (Figure 4A). These functions were averaged between the bed and $H_{umax}$, and transformed to the density difference. $S$ is the tangent of the slope (–). The resulting values of shear velocity are 0.084 m/s for Run 1, and 0.064 m/s for Run 2.

Another measure that is commonly used to evaluate turbulent mixing is the turbulence intensity. The turbulence intensity $I(z)$ (m/s) can be obtained from a time series of velocity measurements as (Kneller *et al.*, 1999; Eggenhuisen and McCaffrey, 2012):

$$I(z) = \sqrt{\overline{u'(t,z)^2}} \tag{8}$$

where the overbar denotes time-averaging, and $u'(t,z)$ are the instantaneous velocity deviations defined as (Eggenhuisen and McCaffrey, 2012):

$$u'(t,z) = u(t,z) - \overline{u(z)} \tag{9}$$

where $u(t,z)$ are the measured time series of instantaneous velocity as a function of distance above the bed (m/s).

## 3 | RESULTS

### 3.1 | Flume experiments

#### 3.1.1 | Suspension samples

The concentration and grain-size stratification profiles from the two experimental currents are presented in Figure

4A,B, respectively. Both runs have concave-up concentration profiles (Figure 4A), although the high-slope run (Run 1) displays a more rapid upward decrease in concentration than the low-slope run (Run 2). In addition, the grain size decreases upwards in the flow in both runs (Figure 4B), yet vertical grain size sorting is most pronounced in the low-slope run.

Figure 5A,B shows the full grainsize distribution of each of the suspended sediment samples collected with the siphoning tubes. The samples from the lower two siphoning tubes (0.01 and 0.02 m above the bed) are enriched in coarse-grained sediment and depleted in fine-grained sediment relative to the composition of the sediment supplied at the inlet. Contrastingly, the samples from the upper two siphoning tubes (0.04 and 0.08 m above the bed) are enriched in fine sediment, and depleted in the coarser sediment, compared with the sediment at the input.

Velocity and turbulence intensity profiles are shown in Figure 6. Time-averaged velocity profiles (Figure 6A) illustrate that current velocity increases with slope. The maximum velocity of the low-slope run is 1.0 m/s while the maximum velocity of the turbidity current in the high-slope run is 1.2 m/s. The turbulence intensity profile (Figure 6B) of the high-slope run displays a turbulence minimum around the velocity maximum, as observed in previous experimental turbidity current studies (Kneller *et al.*, 1999; Eggenhuisen and Mccaffrey, 2012; Cartigny *et al.*, 2013). The low-slope turbidity current shows little vertical variation in turbulence intensity and has a lower turbulence intensity in general.

### 3.2 | Comparison of modelled and experimental results

Figures 7 and 8 show the experimental and analytical modelling results of the high-slope and low-slope run, respectively. Grain-size trends (Figures 7A and 8A) produced by the model are in good agreement with the experimental results. The largest divergences between the modelled and measured results occur towards the top of the current. Moreover, the goodness of fit is not uniform across grain sizes. The gradients of the median grain size ($D_{50}$) and $10^{th}$ size percentile ($D_{10}$) measured in the experiments closely resemble the model results, whereas the model clearly underpredicts the grain size of the $90^{th}$ size percentile ($D_{90}$) of the grain-size distributions (Figures 7A and 8A).

Normalized concentration profiles for different sediment grain-size classes are presented in Figures 7B and 8B. Both model and experiments show that the fine sediment grain-size classes are more uniformly distributed over the height of the flow than the coarse sediment grain-size classes. However, the fit between the model and the experiments is not equally good for the concentration profiles of all grain-size classes. The measured concentration profiles for the coarse sediment grain-size classes (126–142 μm, 159–178 μm and 200–224 μm) are in reasonable agreement with the model. However, the upward decrease in concentration for the finest grain-size class that is plotted (32–36 μm) is severely under predicted by the model. In the high-slope run (Run 1), for example, the model predicts that sediment in the 32–36 μm class is nearly homogeneously distributed over the height of the flow (Figure 7B) while the experimental measurements show a significant upward decrease in concentration.

Concentration profiles produced by the model are also in reasonable agreement with experimental measurements (Figures 7C and 8C), although some differences occur. The concentration profiles predicted by the model are more concave than the measured concentration profiles. Also, the model predicts relatively high concentrations in the upper part of the flow, which is not in agreement with the exponential decay that characterizes the measured concentration profiles.

## 4 | DISCUSSION

### 4.1 | Comparison between nature and experiments

The experimental turbidity currents show a gradual change in suspended sediment grain-size distribution upwards in the flow (Figure 5A,B). The coarse sediment fraction becomes gradually less abundant while the fine sediment fraction gradually becomes more abundant with height. Similar direct measurements of suspension composition at multiple elevations above the bed are currently not available for natural turbidity currents. As a substitute, deposit samples from different elevations above the thalweg of a canyon or channel can be used. Grain-size distributions of deposit samples are available for the levees of the Amazon Channel (Figure 5C) (Hiscott *et al.*, 1997; Manley *et al.*, 1997; Pirmez and Imran, 2003) and for the walls of the Monterey Canyon (Figure 5D) (Symons *et al.*, 2017).

Deposit samples from the Amazon Channel were collected during an ODP cruise (ODP Leg 155). Samples were collected from the channel floor, channel terraces and levee flanks at different distances down channel. Channel relief differed between the locations, and samples thus represent channel overspill at different elevations above the channel thalweg (Hiscott *et al.*, 1997). Figure 5C shows one representative grain-size distribution from each core location. Apart from the channel floor samples, the samples are all dominated by silt-sized sediment. The change in grain-size distribution of the Amazon samples shows a pattern that is similar to the experiments (Figure 5A and B). The fine sediment fraction becomes relatively more abundant with height above the base of the flow while the coarse sediment fraction becomes relatively less abundant.

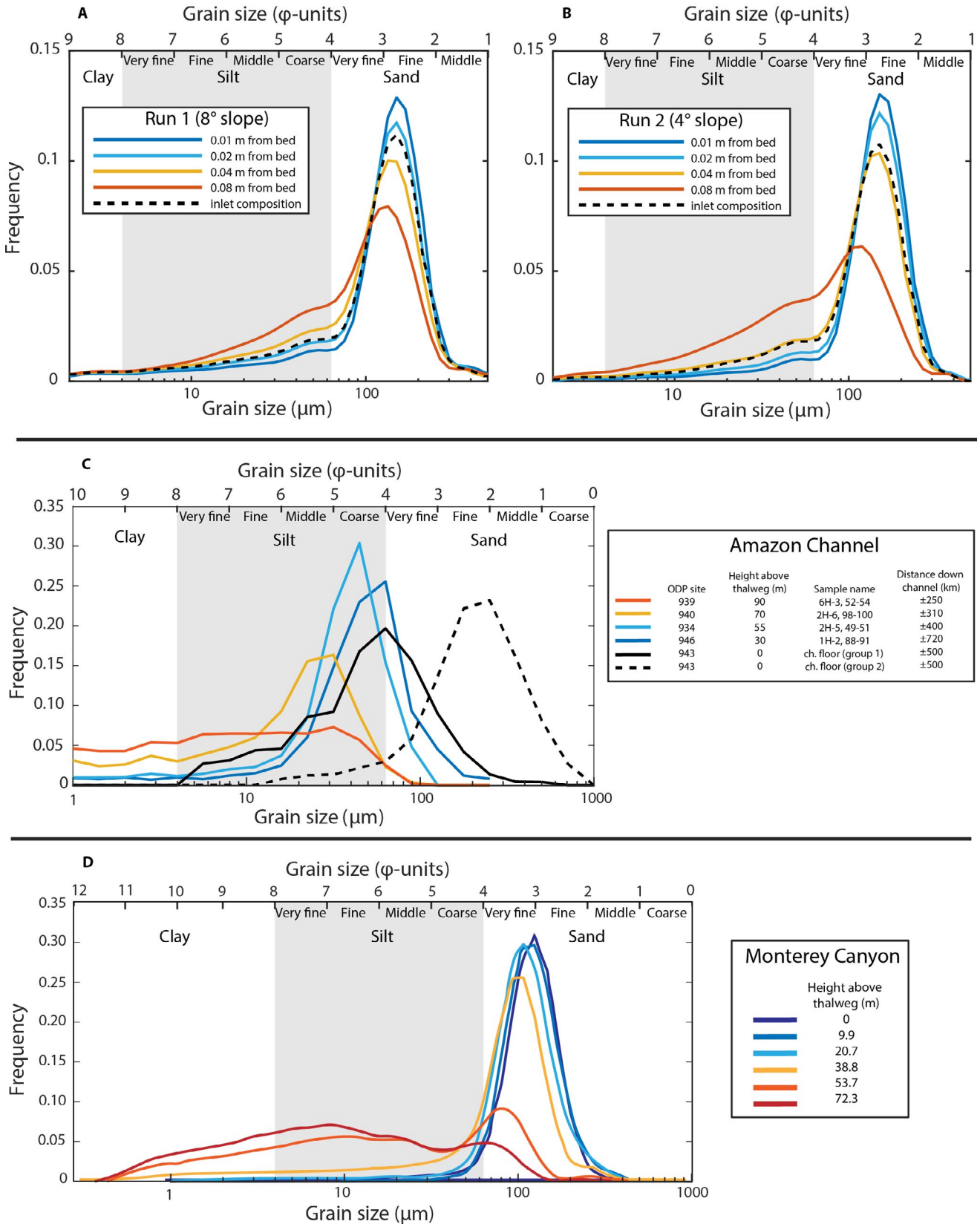


**FIGURE 5** (A, B) Grain-size distribution of suspended sediment samples collected with siphon tubes at different elevations above the bed in experimental turbidity currents. (A) Suspended sediment samples from Run 1 (8° slope). (B) Suspension samples collected during Run 2 (4° slope). (C) Grain-size distribution of deposit samples from the Amazon Channel (Hiscott et al., 1997; Manley et al., 1997). (D) Grain-size distribution of deposit samples from the canyon wall of the Monterey Canyon (Symons et al., 2017). Note that the shift in grain-size distribution with height above the thalweg shows a similar pattern in the natural systems and in the experiments.

Samples in the Monterey Canyon were collected at different heights on the canyon wall and are dominated by sand-sized sediment. Figure 5D shows the grain-size distribution of each of the cores. Again, a gradual shift towards the finer sediment grain-size classes with height above the thalweg is observed.

Published median grain sizes for the Niger slope (Figure 1B; Jobe *et al.*, 2017) and the Var canyon (Figure 1C; Migeon *et al.*, 2012) further corroborate the similarity between experimental results and natural systems. This similarity suggests that grain-size stratification arises in a similar way in experimental turbidity currents and in natural currents, which are orders of magnitude larger, and that the model, having been validated using experiments, can be extended to natural systems which exhibit concentration profiles similar to those observed in the experiments.

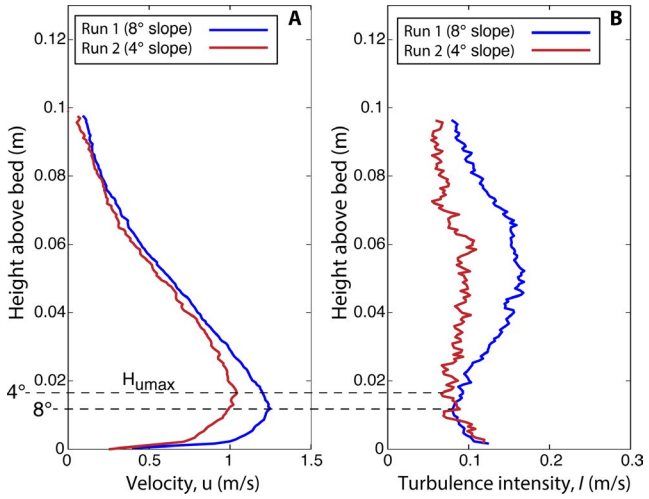


**FIGURE 6** (A) Time-averaged velocity profiles of Run 1 and 2. (B) Turbulence intensity profiles from Runs 1 and 2. Note that the turbidity current on the steeper slope (Run 1) has a higher flow velocity and higher turbulence intensity

## 4.2 | Comparison between experiments and model

The Rousean model performs best for the concentration profiles of fine-grained sand that is predominantly suspended in the lower part of the flow (Figures 7B and 8B). The concentration profiles for very fine-grained sand and, especially, silt, display the largest mismatch between the model and the experiments. This mismatch occurs because modest shear velocity values suffice to homogenously diffuse silt against the pull of gravity over the depth of a current in the Rouse equation (see also Parker *et al.*, 1986). There exists a counter-intuitive relationship between the mismatches in these grain-size-class concentration profiles and the predicted grain-size distributions towards the top of the flow. The latter display significant error by underpredicting $D_{90}$ of the suspension high in the flow. This error is not due to problems in predicting the distribution of coarser material but due to the incorrect prediction of elevated silt content in the upper part of the flow, which reduces the fraction of coarser material and thus draws the 90$^{th}$ percentile of grain size down (Figures 7A and 8A). This error has some consequences for studies using Rousean models to predict the composition of the part of turbidity currents that spills over the levee crest (Straub and Mohrig, 2008; Bolla Pittaluga *et al.*, 2018), which is predicted to be too fine. Conversely, flow strength will be overestimated in inverse approaches that use deposit grain size of channel margin or levee deposits to reconstruct flow characteristics

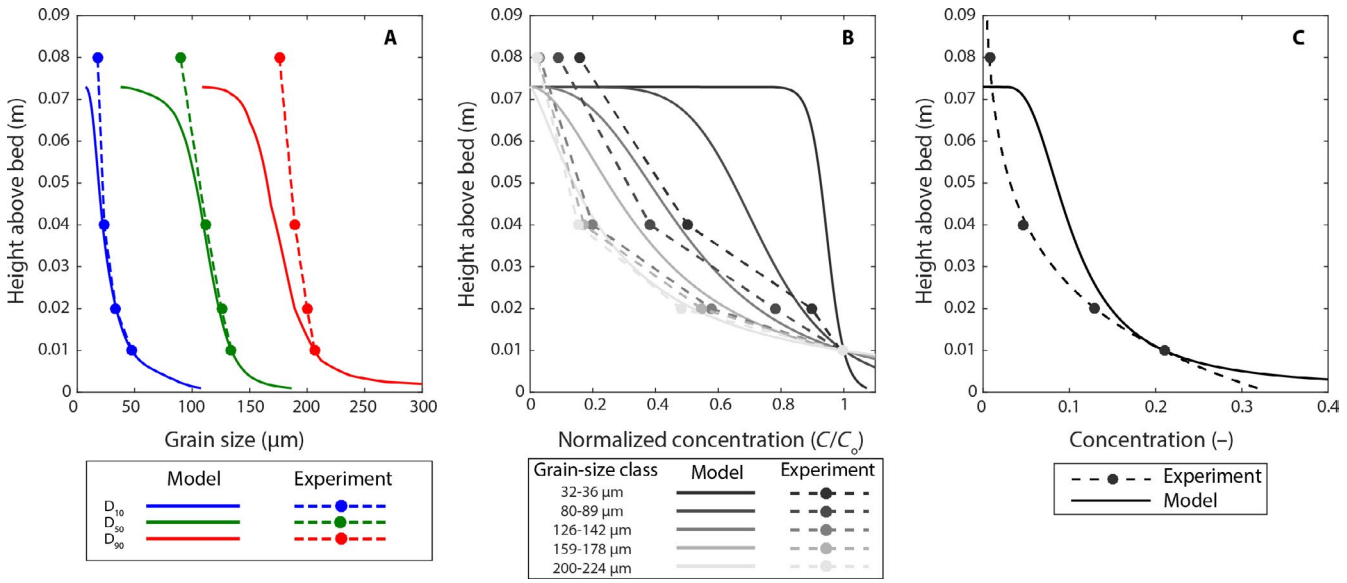


**FIGURE 7** Comparison between results from Run 1 (8° slope) and the results from the analytical model. (A) $D_{10}$, $D_{50}$ and $D_{90}$ profiles. (B) Normalized concentration profiles by grain-size class. (C) Concentration profile

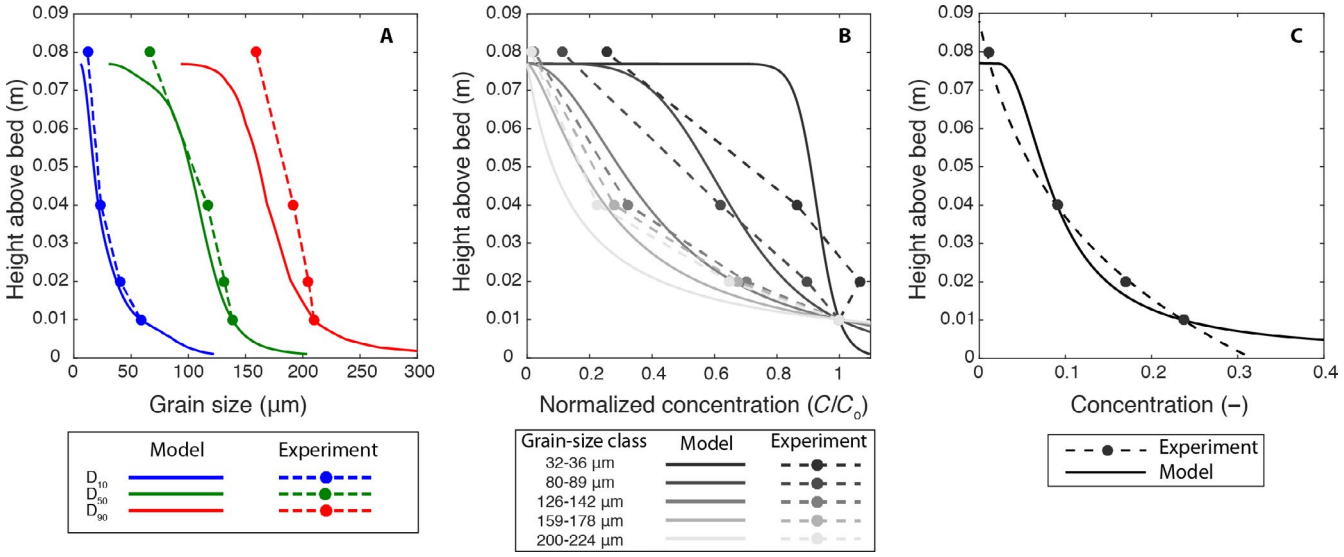


**FIGURE 8** Comparison between results from Run 2 (4° slope) and the results from the analytical model. (A) $D_{10}$, $D_{50}$ and $D_{90}$ profiles. (B) Normalized concentration profiles by grain-size class. (C) Concentration profile

(Hiscott *et al.*, 1997; Jobe *et al.*, 2017; de Leeuw *et al.*, 2018), because $D_{90}$ is systematically underpredicted in the upper part of turbidity currents (Figures 7A and 8A). These issues are much less prominent in the part of the current that is located beneath the velocity inflection point (approximately 4 cm in Figures 6A, 7 and 8), where the majority of sediment is transported. The problems of the Rousean approach are thus less significant when the focus is on the throughput of sand in proximity to the channel floor (Dorrell *et al.*, 2013, 2018; de Leeuw, Eggenhuisen, Spychala, *et al.*, 2018).

In conclusion, the suspended load of turbidity currents can be reasonably modelled using the classic formulation of the Rouse equation, especially when the focus is on the sediment transported beneath the velocity inflection. This conclusion is perhaps not surprising, given that the parabolic diffusivity distribution can be considered to be most appropriate for the lower part of turbidity currents (Altinakar *et al.*, 1996).

### 4.2.1 | Origin of differences between model and experiments

It is possible to identify three processes that may help to further explain the differences between the measured and modelled density structure of the experimental turbidity current, which are most pronounced towards the top of the current: (a) insufficient time to reach an equilibrium structure; (b) inability of the model to capture the feedbacks between turbulence diffusion and the sediment load of the flow and (c) the innate differences between the turbulence structure of open-channel flows and turbidity currents.

First, one of the assumptions behind the Rouse equation is that the sediment distribution in the flow has reached an equilibrium. This assumption may not be valid for the flume experiments because there was only a limited amount of time available between the inlet point and the position where the samples were collected from the flow. Given a distance of 2.35 m and a depth-averaged flow velocity of ~0.7 m/s, the time available for stratification to develop was about 3.5 s. This time period may not have been enough time to establish an equilibrium profile for all grain-size classes. Using an analytical model, Dorrell and Hogg (2012) have shown that the timescale of response of suspensions to changing flow conditions are grain-size dependent and the response time is longer for smaller grain sizes. This difference in response timescale could explain why the finer grain sizes are most poorly predicted by the Rouse equation. Further work is needed to establish the degree to which the concentration profiles in the present experiments resemble a steady state. Such experiments would evaluate the travel distance needed for turbidity currents to develop into a flow structure that qualifies as 'gradually varied flow'.

Second is the assumption that turbulent diffusion is unaffected by the presence of suspended solids. Recent theoretical work on the transition from competency to capacity driven deposition is linked to the gravitational force acting on the suspended mass exceeding the upward turbulent forces near the bed (Eggenhuisen *et al.*, 2017). This work is consistent with numerical investigations that have shown that turbulence suppression is linked to the development of a stably stratified basal layer, which decreases the eddy diffusivity, inhibiting the diffusion of turbulence away from the bed (Cantero *et al.*, 2009, 2011). In addition, new turbulence closure models are addressing a feedback between turbulence characteristics and sediment load, demonstrating that the

ratio between diffusivity of particles and turbulent diffusivity ($\beta$ in Equation 1) varies based on local density gradients (Karimpour and Venayagamoorthy, 2014). In the context of the present study, these advances indicate that $\beta$ should change considerably with distance from the bed in density-stratified turbidity currents, whereas the Rouse equation in its standard formulation assumes that $\beta$ remains constant through the water column, resulting in over-predictions of particle concentration at the base of the flow. Considering that the largest mismatches between experiment and Equation 1 with $\beta \approx 1$ occur at the top of the flow, not at the base (Figures 7 and 8), it is unlikely that the effect of suspended sediment on diffusivity is a major factor inhibiting the application of a simple formulation for the Rouse equation (see also Bolla Pittaluga and Imran, 2014).

The third possible cause of mismatch between simulation and experiment is the difference in the turbulence diffusivity structure between turbidity currents and open-channel flow, which is also the most poorly understood of the three proposed error sources. As previously noted, turbulence diffusion characteristics of clear-water open-channel flow is best described by a parabolic function, where diffusivity reaches its minima at $z = 0$ and $z = H$, whereas the maxima occurs at $z = H/2$. However, turbidity currents are characterized by a composite velocity structure where the region below $u_{max}$ resembles that of open-channel flow, and the mixing layer behaves like a jet structure with rigorous mixing with the overlying ambient fluid, and whose diffusivity characteristics remain constant with depth (Pope, 2000). Importantly, turbulence intensity in the mixing layer increases relative to the turbulence intensity below the velocity maximum in the high-slope run (Figure 6). This increase in turbulence is because as flow velocity increases, so too does the shear between the current and the ambient fluid compared with that of the bed, indicating that the mixing layer becomes more influential in defining the current's turbulence characteristics. More intense mixing leads to more homogenous suspension of sediment and higher bulk sediment concentrations in a simple diffusive model (Figure 2B). This is, however, where we encounter the most fundamental divergence between the open-channel theory and turbidity current reality: more intense mixing in turbidity currents actually leads to lower average sediment concentrations due to the enhanced entrainment of ambient water (Figures 4A and 6). While incorporating the effects of the mixing layer into the Rouse equation would likely improve the modelled results, especially in the upper part of the flow, and for the distribution of silt, to date there is no obvious way to incorporate theory for mixing layer dynamics into an algebraic sediment suspension model. It seems that simple diffusive approaches commonly used in literature will (have to) do while this theoretical challenge is unresolved.

# 5 | CONCLUSIONS

Reconstructing turbidity current events directly from the geologic record represents a commonly used technique for interpreting the factors controlling the evolution of sub-marine channel-levee systems. If successful, this approach can yield valuable insight into fluxes of sediment through submarine canyons and channels. However, simplified modelling approaches have been adopted without thorough validation against measurements. The present study addresses this uncertainty by comparing the measured grain-size stratification characteristics of experimental turbidity currents with datasets for systems in nature and those predicted by a Rousean sediment suspension model.

The Rouse equation accurately models the concentration profiles of fine-grained sand that is predominantly suspended in the lower part of experimental turbidity currents. The concentration profiles of finer grained sediment display the largest mismatch between the model and the experiments, especially in the upper part of the turbidity currents. Rousean models thus seem relatively dependable for simulations of sediment throughput in the lower part of the flow. Caution is advised where the Rouse equation is used to evaluate the upper portion of the flow that spills over levee crests. Inversion of flow characteristics from levee crest deposits with the Rouse equation may lead to overestimation of the turbidity current strength.

It is recognized that there are opportunities to re-parameterize the diffusion component of the Rouse model to better reflect the turbulence properties of turbidity currents. However, these results demonstrate that the standard open-channel flow diffusion model works well as a first-order approximation in defining the concentration and grain-size structure of turbidity currents. As such, reconstructing flow events directly from the geologic record with a Rousean diffusion model is a viable tool in the arsenal of sedimentologists wishing to interpret the evolution of sub-marine channel settings.

## ACKNOWLEDGEMENTS

Henk van der Meer and Thony van der Gon are thanked for technical assistance with the experiments. Zane Jobe, an anonymous reviewer, and associate editor Paul Carling are acknowledged for their comments and suggestions, which helped us to improve the paper. This is a contribution of the Eurotank Studies of Experimental Deepwater Sedimentology (EuroSEDS), financially supported by the Dutch Research Council (NWO; Grant NWO-ALW-VIDI 864.13.006), ExxonMobil, Shell and Equinor.

## CONFLICT OF INTEREST

The authors have no conflict of interest to declare.

## DATA AVAILABILITY STATEMENT

The data that support the findings of this study are available on request from the corresponding author.

## ORCID

*Joris T. Eggenhuisen* https://orcid.org/0000-0002-7389-9665

## REFERENCES

Abd El-Gawad, S., Cantelli, A., Pirmez, C., Minisini, D., Sylvester, Z. and Imran, J. (2012) Three-dimensional numerical simulation of turbidity currents in a submarine channel on the seafloor of the Niger Delta slope. *Journal of Geophysical Research*, *117*, C05026. https://doi.org/10.1029/2011JC007538.

Abd El-Gawad, S.M., Pirmez, C., Cantelli, A., Minisini, D., Sylvester, Z. and Imran, J. (2012) 3-D numerical simulation of turbidity currents in submarine canyons off the Niger Delta. *Marine Geology*, *326–328*, 55–66. https://doi.org/10.1016/j.margeo.2012.06.003.

Altinakar, M.S., Graf, W.H. and Hopfinger, E.J. (1996) Flow structure in turbidity currents. *Journal of Hydraulic Research*, *34*, 713–718. https://doi.org/10.1080/00221689609498467.

Baas, J.H., McCaffrey, W.D., Haughton, P.D.W. and Choux, C. (2005) Coupling between suspended sediment distribution and turbulence structure in a laboratory turbidity current. *Journal of Geophysical Research: Oceans*, *110*, 1–20. https://doi.org/10.1029/2004JC002668.

Babonneau, N., Savoye, B., Cremer, M. and Bez, M. (2010) Sedimentary architecture in meanders of a submarine channel: detailed study of the present Congo turbidite channel (Zaiango Project). *Journal of Sedimentary Research*, *80*, 852–866. https://doi.org/10.2110/jsr.2010.078.

Bolla Pittaluga, M. and Imran, J. (2014) A simple model for vertical profiles of velocity and suspended sediment concentration in straight and curved submarine channels. *Journal of Geophysical Research: Earth Surface*, *119*, 483–503. https://doi.org/10.1002/2013JF002812.Received.

Bolla Pittaluga, M., Frascati, A. and Falivene, O. (2018) A gradually varied approach to model turbidity currents in submarine channels. *Journal of Geophysical Research: Earth Surface*, *123*, 80–96. https://doi.org/10.1002/2017JF004331.

Cantero, M.I., Balachandar, S., Cantelli, A., Pirmez, C. and Parker, G. (2009) Turbidity current with a roof: direct numerical simulation of self-stratified turbulent channel flow driven by suspended sediment. *Journal of Geophysical Research*, *114*, 1–20. https://doi.org/10.1029/2008JC004978.

Cantero, M.I., Cantelli, A., Pirmez, C., Balachandar, S., Mohrig, D., Hickson, T.A. *et al.* (2011) Emplacement of massive turbidites linked to extinction of turbulence in turbidity currents. *Nature Geoscience*, *5*, 42–45. https://doi.org/10.1038/ngeo1320.

Cartigny, M.J.B., Eggenhuisen, J.T., Hansen, E.W.M. and Postma, G. (2013) Concentration-dependent flow stratification in experimental high-density turbidity currents and their relevance to turbidite facies models. *Journal of Sedimentary Research*, *83*, 1046–1064. https://doi.org/10.2110/jsr.2013.71.

Dennielou, B., Huchon, A., Beaudouin, C. and Berné, S. (2006) Vertical grain-size variability within a turbidite levee: autocyclicity or allocyclicity? A case study from the Rhone neofan, Gulf of Lions, Western Mediterranean. *Marine Geology*, *234*, 191–213. https://doi.org/10.1016/j.margeo.2006.09.019.

Dorrell, R.M. and Hogg, A.J. (2012) Length and time scales of response of sediment suspensions to changing flow conditions. *ASCE Journal of Hydraulic Engineering*, *138*, 430–439. https://doi.org/10.1061/(ASCE)HY.1943-7900.

Dorrell, R.M., Hogg, A.J. and Pritchard, D. (2013) Polydisperse suspensions: erosion, deposition, and flow capacity. *Journal of Geophysical Research-Earth Surface*, *118*, 1939–1955. https://doi.org/10.1002/jgrf.20129.

Dorrell, R.M., Amy, L.A., Peakall, J. and McCaffrey, W.D. (2018) Particle size distribution controls the threshold between net sediment erosion and deposition in suspended load dominated flows. *Geophysical Research Letters*, *45*, 1443–1452. https://doi.org/10.1002/2017GL076489.

Eggenhuisen, J.T. and Mccaffrey, W.D. (2012) The vertical turbulence structure of experimental turbidity currents encountering basal obstructions: implications for vertical suspended sediment distribution in non-equilibrium currents. *Sedimentology*, *59*, 1101–1120. https://doi.org/10.1111/j.1365-3091.2011.01297.x.

Eggenhuisen, J.T., Cartigny, M.J.B. and de Leeuw, J. (2017) Physical theory for near-bed turbulent particle suspension capacity: earth Surface. *Dynamics*, *5*, 269–281. https://doi.org/10.5194/esurf-5-269-2017.

Ellison, T.H. and Turner, J.S. (1959) Turbulent entrainment in stratified flows. *Journal of Fluid Mechanics*, *6*, 423–448. https://doi.org/10.1017/S0022112059000738.

Garcia, M.H. (1994) Depositional turbidity currents laden with poorly sorted sediment. *Journal of Hydraulic Engineering*, *120*, 1240–1263.

Garcia, M. (2008) Sedimentation engineering: processes, measurements, modeling, and practice. ASCE.

Graf, W.H. (1971) *Hydraulics of sediment transport. Water Resources Publications*, Colorado, USA, pp 513.

Hansen, L.A.S., Callow, R.H.T., Kane, I.A., Gamberi, F., Rovere, M., Cronin, B.T. *et al.* (2015) Genesis and character of thin-bedded turbidites associated with submarine channels. *Marine and Petroleum Geology*, *67*, 852–879. https://doi.org/10.1016/j.marpetgeo.2015.06.007.

Hiscott, R.N. (1994) Loss of capacity, not competence, as the fundamental process governing deposition from turbidity currents. *Journal of Sedimentary Research*, *64*, 209–214.

Hiscott, R.N., Hall, F.R. and Pirmez, C. (1997) Turbidity-current overspill from the Amazon Channel: texture of the silt/sand load, paleoflow from anisotropy of magnetic susceptibility and implications for flow processes. *Proceedings of the Ocean Drilling Porgram, Scientific Results*, *155*, 53–78. https://doi.org/10.2973/odp.proc.sr.155.202.1997.

Huang, H., Imran, J. and Pirmez, C. (2007) Numerical modeling of poorly sorted depositional turbidity currents. *Journal of Geophysical Research: Oceans*, *112*, 1–15. https://doi.org/10.1029/2006JC003778.

Hubbard, S.M., Covault, J.A., Fildani, A. and Romans, B.W. (2014) Sediment transfer and deposition in slope channels: deciphering the record of enigmatic deep-sea processes from outcrop. *Geological Society of America Bulletin*, *126*, 857–871. https://doi.org/10.1130/B30996.1.

Jobe, Z., Sylvester, Z., Pittaluga, M.B., Frascati, A. and Pirmez, C. (2017) Facies Architecture of submarine channel deposits on the Western Niger Delta Slope : implications for grain-size and density stratification in turbidity currents. *Journal of Geophysical Research*, *122*, 473–491.

Kane, I.A. and Hodgson, D.M. (2011) Sedimentological criteria to differentiate submarine channel levee subenvironments: exhumed examples from the Rosario Fm. (Upper Cretaceous) of Baja California, Mexico, and the Fort Brown Fm. (Permian), Karoo Basin, S. Africa. *Marine and Petroleum Geology*, *28*, 807–823. https://doi.org/10.1016/j.marpetgeo.2010.05.009.

Karimpour, F. and Venayagamoorthy, S.K. (2014) A simple turbulence model for stably stratified wall-bounded flows. *Journal of Geophysical Research: Oceans*, *119*, 870–880. https://doi.org/10.1002/2013JC009332.

Kneller, B. (2003) The influence of flow parameters on turbidite slope channel architecture. *Marine and Petroleum Geology*, *20*, 901–910. https://doi.org/10.1016/j.marpetgeo.2003.03.001.

Kneller, B. and Buckee, C. (2000) The structure and fluid mechanics of turbidity currents: a review of some recent studies and their geological implications. *Sedimentology*, *47*, 62–94. https://doi.org/10.1046/j.1365-3091.2000.047s1062.x.

Kneller, B.C., Bennett, S.J. and McCaffrey, W.D. (1999) Velocity structure, turbulence and fluid stresses in experimental gravity currents. *Journal of Geophysical Research*, *104*, 5381. https://doi.org/10.1029/1998JC900077.

de Leeuw, J., Eggenhuisen, J.T. and Cartigny, M.J.B. (2018) Linking submarine channel–levee facies and architecture to flow structure of turbidity currents: insights from flume tank experiments. *Sedimentology*, *65*, 931–951. https://doi.org/10.1111/sed.12411.

de Leeuw, J., Eggenhuisen, J.T., Spychala, Y.T., Heijnen, M.S., Pohl, F. and Cartigny, M.J.B. (2018) Sediment volume and grain-size partitioning between submarine channel-levee systems and lobes: an experimental study. *Journal of Sedimentary Research*, *88*, 777–794. https://doi.org/10.2110/jsr.2018.46.

Manley, P. L., Pirmez, C., Busch, W., & Cramp, A. (1997) Grain-size characterization of Amazon Fan deposits and comparison to seismic facies units. *Proceedings of the Ocean Drilling Porgram, Scientific Results*, *155*, 35–52.

Migeon, S., Mulder, T., Savoye, B. and Sage, F. (2012) Hydrodynamic processes, velocity structure and stratification in natural turbidity currents: results inferred from field data in the Var Turbidite System. *Sedimentary Geology*, *245-246*, 48–62. https://doi.org/10.1016/j.sedgeo.2011.12.007.

Parker, G., Fukushima, Y. and Pantin, H.M. (1986) Self-accelerating turbidity currents. *Journal of Fluid Mechanics*, *171*, 145–181. https://doi.org/10.1017/S0022112086001404.

Paull, C. K., Ussler III, W., Caress, D. W., Lundsten, E., Covault, J. A., Maier, K. L. *et al*. (2010) Origins of large crescent-shaped bedforms within the axial channel of Monterey Canyon, offshore California. *Geosphere*, *6*, 755–774. https://doi.org/10.1130/GES00527.1.

Pirmez, C. and Imran, J. (2003) Reconstruction of turbidity currents in Amazon Channel. *Marine and Petroleum Geology*, *20*, 823–849. https://doi.org/10.1016/j.marpetgeo.2003.03.005.

Pohl, F., Eggenhuisen, J.T., Cartigny, M.J.B., Tilston, M.C., de Leeuw, J. and Hermidas, N. (2019) The influence of a slope break on turbidite deposits: an experimental investigation. *EarthArXiv*. June 24, https://doi.org/10.31223/osf.io/v58gm

Pope, S.B. (2000) *Turbulent flows*. Cambridge, UK: Cambridge University Press, 771 pp.

van Rijn (1993) *Principles of sediment transport in rivers, estuaries and coastal seas*. Aqua Publications, Amsterdam, the Netherlands, pp. 715.

Rouse, H. (1937) Modern conceptions of the mechanics of fluid turbulence. *Transactions of the American Society of Civil Engineers*, *102*, 463–505.

Sequeiros, O.E., Mosquera, R. and Pedocchi, F. (2018) Internal structure of a self-accelerating turbidity current. *Journal of Geophysical Research: Oceans*, *123*, 6260–6276. https://doi.org/10.1029/2018JC014061.

Stacey, M. and Bowen, A. (1988) The vertical structure of density and turbidity currents: theory and observations. *Journal of Geophysical Research*, *93*, 3528–3542. https://doi.org/10.1029/JC093iC04p03528.

Straub, K.M. and Mohrig, D. (2008) Quantifying the morphology and growth of levees in aggrading submarine channels. *Journal of Geophysical Research: Earth Surface*, *113*, 1–20. https://doi.org/10.1029/2007JF000896.

Straub, K.M., Mohrig, D., Buttles, J., McElroy, B. and Pirmez, C. (2011) Quantifying the influence of channel sinuosity on the depositional mechanics of channelized turbidity currents: a laboratory study. *Marine and Petroleum Geology*, *28*, 744–760. https://doi.org/10.1016/j.marpetgeo.2010.05.014.

Symons, W.O., Sumner, E.J., Paull, C.K., Cartigny, M.J.B., Xu, J.P., Maier, K.L. *et al*. (2017) A new model for turbidity current behavior based on integration of flow monitoring and precision coring in a submarine canyon. *Geology*, *45*, 367–370. https://doi.org/10.1130/G38764.1.

Tilston, M., Arnott, R.W.C., Rennie, C.D. and Long, B. (2015) The influence of grain size on the velocity and sediment concentration profiles and depositional record of turbidity currents. *Geology*, *43*, 839–842. https://doi.org/10.1130/G37069.1.

Vanoni, V.A. (1946) Transportation of suspended sediment by water. *Transactions of the American Society of Civil Engineers*, *111*(1), 67–102.

Vanoni, V.A. (2006) *Sedimentation Engineering*. ASCE Manual of Practice. Vol. 54, no. 110, 1–431. https://doi.org/10.1061/9780784408230.

**How to cite this article:** Eggenhuisen JT, Tilston MC, de Leeuw J, Pohl F, Cartigny MJB. Turbulent diffusion modelling of sediment in turbidity currents: An experimental validation of the Rouse approach. *Depositional Rec*. 2020;6:203–216. https://doi.org/10.1002/dep2.86